Provided for non-commercial research and education use.
Not for reproduction, distribution or commercial use.

This article appeared in a journal published by Elsevier. The attached copy is furnished to the author for internal non-commercial research and education use, including for instruction at the authors institution and sharing with colleagues.

Other uses, including reproduction and distribution, or selling or licensing copies, or posting to personal, institutional or third party websites are prohibited.

In most cases authors are permitted to post their version of the article (e.g. in Word or Tex form) to their personal website or institutional repository. Authors requiring further information regarding Elsevier's archiving and manuscript policies are encouraged to visit:

http://www.elsevier.com/copyright

Author's personal copy

Thin Solid Films 522 (2012) 452–456

Contents lists available at SciVerse ScienceDirect

Thin Solid Films

journal homepage: www.elsevier.com/locate/tsf

Surface plasmon resonance investigation procedure as a structure sensitive method for SnO_2 nanofilms

V.S. Grinevich [b,*], L.M. Filevska [b], I.E. Matyash [a], L.S. Maximenko [a], O.N. Mischuk [a], S.P. Rudenko [a], B.K. Serdega [a], V.A. Smyntyna [b], B. Ulug [c]

[a] V. Lashkaryov Institute of Semiconductor Physics, National Academy of Sciences of Ukraine, 45 Nauky Prospect, 03028 Kiev, Ukraine
[b] Odessa I.I. Mechnikov National University, 2 Dvoryanska St., 65082 Odessa, Ukraine
[c] Akdeniz University, Department of Physics, Faculty of Science, Antalya, Turkey

ARTICLE INFO

Article history:
Received 11 July 2011
Received in revised form 28 August 2012
Accepted 29 August 2012
Available online 8 September 2012

Keywords:
Surface plasmon resonance
Tin dioxide
Thin films

ABSTRACT

General principles of the surface plasmon resonance (SPR) phenomenon are applied to studying the structure and physical properties of thin conducting tin dioxide (SnO_2) films. The SPR effects are detected and investigated by the methods of polarization modulation of the incident electromagnetic radiation. Angular and spectral dependencies of the reflection coefficients R_s^2 and R_p^2 for the s- and p-polarized radiation, together with their polarization difference $\rho = R_s^2 - R_p^2$ are measured in the wavelength range of 400–1600 nm. Experimentally obtained $\rho(\theta, \lambda)$ characteristics reflect the peculiar optical properties associated with the film structure and morphology. Surface plasmon–polaritons and local plasmons excited by s- and p-polarized radiation were observed. The results confirm that the SPR technique is a sensitive and informative method for the analysis of the SnO_2 film structure.

© 2012 Elsevier B.V. All rights reserved.

1. Introduction

Investigation of thin films of tin dioxide (SnO_2) is motivated by their numerous applications as a transparent material for electrodes, in gas sensors, as a catalyst in oxidation processes [1–3]. A diversity of properties of SnO_2 surface is caused by an ability of Sn to be in two different oxidation states, Sn^{4+} and Sn^{2+} [1]. As a result, reversible transformations of SnO_2 surface composition occur between stoichiometric Sn^{4+} and reduced Sn^{2+}, depending on the oxygen chemical potential in a system. Surface reduction modifies SnO_2 electronic structure with a formation of the Sn 5s configuration; electronic energy levels of which lie deeply in the bandgap. It provides reducing of electronic work function and an appearance of free carriers. The working model of the present investigation was formulated with regard to the above properties of tin oxide thin films.

It is known that the surface plasmon resonance (SPR) effect can provide information about an arrangement of metal structures in which SPR is observed. It is traditionally considered that SPR is inherent for such metals as silver, gold, aluminum, and copper, for which the dielectric constant is negative (the refractive index $n<1$) in the visible range [4,5]. The SPR effect for metal films is usually observed by means of the reflection coefficient measurements with the use of the well-known Otto [6] or Kretschman [7] optical schemes.

Reflection coefficients of the mostly often investigated metals (gold, silver, aluminum, copper) are rather high. For other materials possessing lower reflection coefficients a different method of SPR detection can be used which is based on the investigation of the optical anisotropic effects [8]. In this method the incident light is subjected to the modulation of the polarization [9]. The experimentally measured parameter in this method is the polarization difference ρ of the reflection coefficients, where $\rho = R_s^2 - R_p^2$ and R_s, R_p are the polarization reflection coefficients for the light polarized perpendicularly or in parallel to the plane of the incidence, respectively. High sensitivity of the parameter ρ to the morphology of films deposited on light reflecting surface was demonstrated in [8] where ρ was investigated, as a function of the angle of incidence θ, wavelength of light λ, and the film thickness d under the conditions of total internal reflection.

Therefore, the polarization modulation (PM) method, which consists in the determination of the parameter $\rho(\theta, \lambda, d)$, enables one to extract the information concerning the optical properties of the deposited materials as well as their morphological and structural peculiarities [8,10]. The $\rho(\theta, \lambda, d)$ dependencies are especially informative in case of using the total internal reflection scheme. However, this information can be extracted only after the elaboration of a suitable model allowing proper interpretation of the obtained data.

The films consisting of isolated particles or clusters of particles have certain advantages over the continuous films in the case of their investigation by the PM method. In particular, a curvature of the particles' surface results in a cancelation of the optical transition forbiddance related to the difference of the wave vectors under interaction of light

* Corresponding author. Tel./fax: +380 48 731 74 03.
E-mail addresses: grinevich@onu.edu.ua (V.S. Grinevich), lfilevska@gmail.com (L.M. Filevska), bserdega@isp.kiev.ua (B.K. Serdega), bulentulug@gmail.com (B. Ulug).

0040-6090/$ – see front matter © 2012 Elsevier B.V. All rights reserved.
http://dx.doi.org/10.1016/j.tsf.2012.08.054

Author's personal copy

irradiance with plasmonic excitation in films [11]. Moreover, as it was established by the authors earlier [12], the restriction for the initial state of polarization is removed also because not only p-polarized, but also s-polarized light can excite SPR in a cluster film.

The investigations of SPR in films of metal nanoclusters and nanocomposites, such as Al, Au, indium tin oxide in dielectric matrices of oxides such as WO_3, SnO_2 and TiO_2 are well described in the literature [13–15]. In the present work nanostructured tin dioxide films are considered as nanocomposite structures, which are formed by clusters of nonstoichiometric tin dioxide (SnO_x) in the dielectric matrix of stoichiometric SnO_2. We demonstrate that an application of the PM method followed by an interpretation procedure based on the working model helps one to understand the optical and morphological properties of such composite structures.

2. Sample preparation and experimental techniques

Samples for the investigation were prepared by the technique described in detail in [16]. Bis(acetylacetonato)dichlorotin (BADCT) was used as a tin dioxide precursor [17]. Freshly prepared BADCT was dissolved in acetone at different concentrations, then equal volumes of each solution were mixed with the same volumes of polyvinyl acetate (PVAC) solutions in acetone prepared at different concentrations. The mixtures were then sprayed onto the microscope cover glass of 22×22 mm^2 size. Samples were kept at room temperature for about 15 min to allow the acetone removal prior to annealing them at 600 °C for 6 h in air to achieve the thermal decomposition of the film organic components (BADCT and PVAC) and subsequent removing decay products. The organic component removal was confirmed by our thermogravimetric studies of the precursor [17] and by the data on the PVAC decomposition at temperatures above 200 °C, particularly in the presence of catalytic oxides (tin dioxide in our case) [18]. After annealing, the tin dioxide film was left on the substrate. PVAC was employed to structurize the film during the removal of its decay products.

The samples principle parameters are presented in Table 1. Surface morphology and an average thickness (with an error of about 2%) of the tin dioxide layers were studied by the Atomic Force Microscopy (AFM) method (NanoScope IIIa, Digital Instruments). The tapping mode measurements were carried out with use of a silicon probe with nominal radius of about 10 nm. The investigated surface area was 1000×1000 nm^2.

The AFM phase topology image of the sample T4.P1 (4 wt.% BADCT and 1 wt.% PVAC in the initial solution) is shown in Fig. 1a. Fourier analysis of the sample surface profile enables one to construct a histogram of the characteristic size distribution (Fig. 1b). It is seen that the film consists of two groups of clusters, each occupies approximately equal space on the histogram. One of them contains clusters of several nanometers to 200 nm, the other covers the sizes over 200 nm. Such structural peculiarities of the films can influence the film spectral characteristics. Indeed, the clusterized structure of the film, which contains a considerable number of defects (crystallite and cluster interfaces), should contribute to the formation of an electron plasma after light absorption by the films. At the same time the nanocluster-based structure of the films is responsible for the electronic energy structure and should result in the formation of a large number of the charge carrier traps.

Table 1
The principal parameters of the samples: thickness and the content of the main components in the initial solution.

Sample name	d, nm	BADCT[a]	PVAC[a]
T4.P1	230–400	4	1
T4.P0.5	420	4	0.5
T2.P0.1	350	2	0.1
T2.P2	160	2	2
T0.5.P0.1	80–100	0.5	0.1

[a] The content in the initial solution, wt.%.

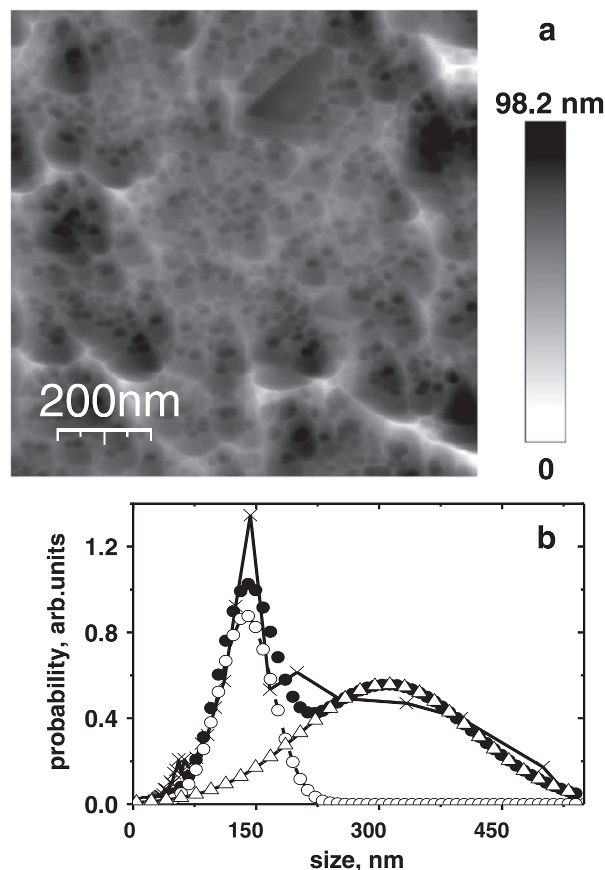

Fig. 1. The phase AFM image of the sample T4.P1 (a) and the cluster size distribution histogram of the film (b).

The experimental setup used in the present work is shown in Fig. 2. The samples were placed on the reflective surface of a total internal reflection prism (half-cylinder) made of melted quartz with refractive index n = 1.45 that results in the critical angle θ_{cr} of 42°. The light source consisted of a combination of an incandescent lamp and a monochromator with the Arens prism placed at the output slit. Internal reflection coefficients R_s^2 and R_p^2 for radiation polarized perpendicularly and in parallel (s-and p-polarization, respectively) relative to the plane of incidence were measured. The value $\rho = R_s^2 - R_p^2$ was calculated as a function of the angle of incidence in one

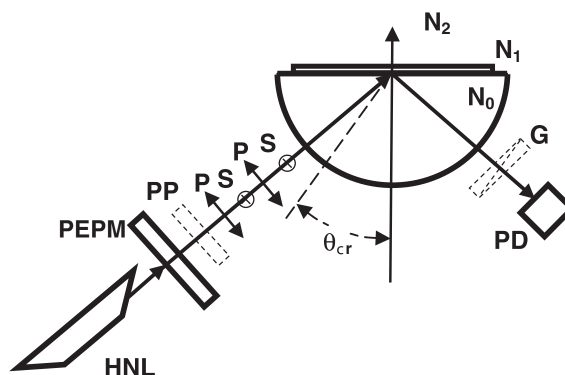

Fig. 2. Experimental setup: HNL — helium-neon laser, PEPM — photoelastic polarization modulator, PP — phase plate, P, S — linear polarizers with polarization directions being parallel and perpendicular to the light incidence plane, G — Glann prism, FD — photo detector, θ_{cr} — critical angle for the total internal reflection, N_0, N_1, and N_2 — the refraction indices of the glass, film, and air, respectively.

Author's personal copy

case and of the wavelength in the range 400–1600 nm in another. Modulated polarized light was used for the measurements of the above dependencies as it is described in details in [8]. The sample was alternatively illuminated by the s- and p-polarized light of the same maximum intensity and optical frequency. To this purpose, the polarization modulator was placed in front of the sample and operated as a quarter wave phase plate. Thus, the constant intensity of circularly polarized radiation was converted into the periodically altered linear one, with electric field being either parallel or perpendicular to the half-cylinder axis. In this case, the measured signal registered at the modulation frequency was proportional to the difference between contributions of the s- and p- polarizations, each depending on the wavelength (the photon energy) and the angle of reflection. The measurements were reliable even when the difference was less than the noise level for each of the functions R_s^2 and R_p^2, and, especially, less than the temporal instability of signals registered separately. At a high frequency modulation ($\omega = 60$ kHz) the low frequency noises characterized by the $1/\omega$ frequency dependence are blocked. Besides, practically simultaneous measuring of the components R_s^2 and R_p^2 eliminates the error of the ρ parameter measurements due to the long-time instability, which accompanies the consecutive component measurement. Thus, during one modulation period, the reflected light gave the difference of orthogonally polarized intensities that was transformed by a photodetector into an alternating signal. This signal was registered by a selective amplifier equipped with a phase-lock detector (lock-in-voltmeter) tuned to the modulation frequency. Hence, a subtraction was performed by the device itself, contrary to the mathematical subtraction procedure where errors are added up and may exceed the extraction result. A linear polarizer added to the system provided measuring the reflection coefficients R_p^2 and R_s^2. For this aim the linear polarizer was placed after the modulator so that in one case its axis coincided with the half-cylinder axis, and was perpendicular to it in another case. During the operation, the polarizer played the role of a 'window', which provides an alternating signal for the photo detector variably transmitting light of a certain polarization. Identification of the s-and p-polarization was performed for the ratio of reflected signals obtained from the clean reflective surface of the half cylinder. Following the Fresnel formulas, this ratio satisfies the condition $R_s^2 \geq R_p^2$ in the whole angular range below the critical angle, that is at $\theta < \theta_{cr}$.

It is worth noting that the parameter ρ sign depends on the values of its constituents and may be negative. This takes place for an "anomalous" reflection when $R_s^2 < R_p^2$, that occurs when the angle of incidence is larger than a critical angle, θ_{cr}. Since the measurements were carried out with a use of lock-in-nanovoltmeter, the parameter ρ real sign was determined on the basis of measurements of the reflection from the clean surface of the half cylinder where the relation $R_s^2 \geq R_p^2$ holds true.

3. Results and discussion

The results obtained will be discussed in terms of the Fresnel formulas describing the reflection indexes R_s^2 and R_p^2 (and, therefore, ρ) as a function of the incident angle θ. Such equation was obtained by the matrix algebra methods applied to a three-layer model "glass–film–air" in which the clusterized film is considered to be flat and homogeneous and describable by the effective optical parameters [8]. This approach is based on the AFM results which show that the films have a smooth surface (that is the film roughness is much smaller than the film thickness). The sample structural heterogeneity is, also, not an obstacle for the film dielectric property characterization by effective optical parameters because the cluster dimensions are much smaller than the wavelengths of the radiation used. Fig. 3a shows the experimental data on dependencies of R_s^2, R_p^2, and ρ on θ for the sample T4.P1 (4 wt.% BADCT and 1 wt.% PVAC in the initial solution) together with the theoretical estimations. The parameters

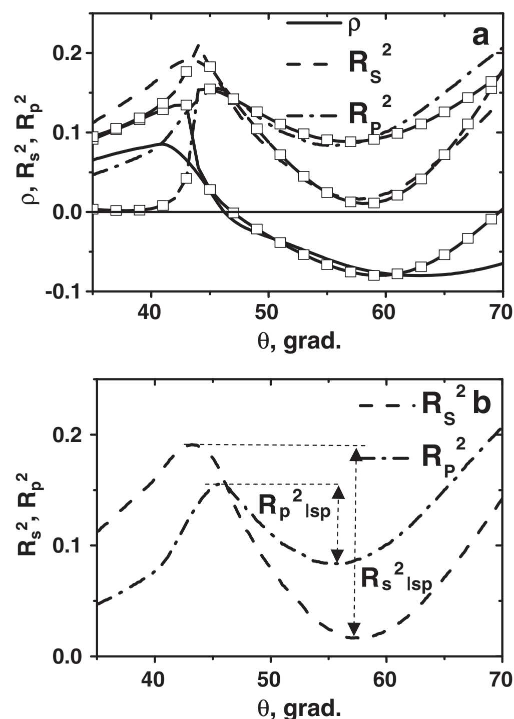

Fig. 3. a) Experimental dependencies (lines) of the internal reflection coefficients $R_s^2(\theta)$, $R_p^2(\theta)$ and the parameter ρ (θ) obtained for the sample T4.P1 in comparison with calculated characteristics (dots). The calculation was performed for the following parameters: $\lambda = 500$ nm; $N = n + I \cdot k$; $n = 1.61$; $k = 0.1$; $d_p = 290$ nm; $d_s = 300$ nm; b) An illustration of different degrees of resonance interaction of the differently polarized light with the film structures of the sample T4.P1 in terms of experimental ${R_s}^2{}_{|sp}$ and ${R_p}^2{}_{|sp}$ dependencies on the light incidence angle.

d_s and d_p used for the calculations are the effective film thicknesses for corresponding polarizations. (The choice of the 500-nm wavelength of the incident light will be justified later.) It should be noted that the narrow angular peak and the sharp fall of $R_p^2(\theta)$ curve are the characteristics of the SPR in metal films.

The figure shows that the typical features of the SPR manifest themselves not only in the $R_p^2(\theta)$, but also in the $R_s^2(\theta)$ curve (downfall at $\theta > \theta_{cr} = 42°$). The fact that such a drop of the $R_s^2(\theta)$ function is wider (in terms of θ) than the one observed for uniform metal films does not contradict the SPR phenomenon nature for the objects of spherical or similar form [11]. The matter is that the incidence angle θ in this case should be measured relatively not to the film surface, but to the plane that is a tangent to the cluster surface and is, therefore, at a certain angle relative to the film plane.

The refractive index and absorption coefficient values for the tin dioxide cluster films, which are necessary for calculations of the coefficients R_s^2, R_p^2 and ρ, were obtained by means of multiparameter fitting of the calculated curves to the experimental ones. It should be stressed that the agreement between the theoretically calculated and experimentally measured data was obtained due to an artificial procedure in which the modified Fresnel formulas were used. The modification was based on the fact that in the cluster films, in contrast to the uniform ones, the s-polarized wave contains the component normal to the surface of a cluster. Formally this fact was taken into account by using different sample thicknesses for the waves possessing orthogonal polarizations.

An applicability of such approach is consistent with the idea of structural anisotropy, which has been mentioned in [10]. It might be expected that increasing the number of fitting parameters (by addition of one more, which is unknown) should complicate the fitting process. However, it was found experimentally that the range of the parameter variations in the course of the fitting procedure was less

Author's personal copy

than 0.2%. Thus, if the film thickness was known, it was not difficult to carry out the fitting procedure by fitting the film refractive indexes and absorption coefficients within their limited ranges of variations.

The optical constants appear to be in agreement with the data presented in [19]. The disagreement between the theoretical and experimental angular dependencies may be explained by the fact that the film, being slightly cuneal, is non-uniform within the light spot area and the latter increases with the angle. Besides, the cluster shape is not spherical that could be taken into account by an additional condition, but, nevertheless, the agreement of the theoretical and experimental data presented in Fig. 3a is quite satisfactory.

An unexpected conclusion, at first glance, can be drawn from Fig. 3a that the SPR phenomenon in metal-dielectric cluster films might be also registered via the surface plasmon excitation by the unpolarized radiation. However, as it was shown above, due to the cluster nonspherical shape the resonance interaction of the clusters with radiation takes place not only for the p-polarized light, as in the case of continuous uniform metal films, but also for the s-polarized light.. Moreover, if one will take into account that the intensity of the resonance interactions manifests itself by the maximum values of the reflection coefficients, it might be concluded from the inequality $R_s^2{}_{|sp} > R_p^2{}_{|sp}$ in Fig. 3(b) that the cluster shape and/or their dielectric environment constitute more preferable conditions for the SPR occurrence under illumination by the s-polarized light. This condition is the phase synchronism relation [5]

$$\sqrt{\varepsilon_0}\,\sin\theta_{sp} = \sqrt{\frac{\varepsilon_2\varepsilon_1(\omega)}{\varepsilon_2+\varepsilon_1(\omega)}}. \quad (1)$$

Here ε_0, $\varepsilon_1(\omega)$, and ε_2 are the real parts of the complex dielectric permittivity of the prism material, metal film and the external environment, respectively. The Eq. (1) expresses the equality of the two components: the metal film projection of the wave vector k_0 of the radiation propagating in the prism at the resonance angle θ_{sp} (left-hand side) and the wave vector k_{sp} of the plasmon wave propagating along the metal surface (right-hand side). In the relation (1) one of its parameters, namely θ_{sp}, being an argument of ρ (θ), illustrates the possibility of excitation of the surface plasmon wave in a wide range of the incident angles due to the non-planar surface of the clusters. The resonant character of the interaction is also evidenced by the ρ (λ) behavior for the samples possessing different thicknesses and tin dioxide concentrations (Fig. 4). It becomes clear from Fig. 4a why the wavelength of 500 nm is used for the angular dependence ρ (θ) shown in Fig. 3 for the sample T4.P1 (4 wt.% BADCT and 1 wt.% PVAC in the initial solution). It is seen that for all samples in the range of 400–500 nm the curves $\rho(\lambda)$ exhibit an extremum. The negative sign of the curves indicates that $R_s^2 < R_p^2$, and, accordingly, testifies for the excitation of surface plasmons both by s- and p-polarized light. This is consistent with the angular dependences shown in Fig. 3 both for R_s^2 and R_p^2 curves and for the polarization difference. Moreover, the magnitude and the sign of the parameter ρ correlate with the sample thickness and SnO_2 content in the initial solutions. Correlating the samples' parameters with the magnitude and the sign of the polarization difference ρ shows that the growth of the SnO_2 concentration is accompanied by a decrease of the ρ value. The T2.P2 sample data are not shown in the set of dependencies in Fig. 4a because this curve, occupying an intermediate position between the negative and positive curves, completely coincides with the horizontal axis. The presence in the investigated films of the resonance interaction of another type is evidenced by the $\rho(\lambda)$ dependencies demonstrated in the Fig. 4b for the two samples in the extended wavelength range. One of the curves shows an extremum at $\lambda \cong 950$ nm that is typical for the resonance effect, in the second curve one can observe only the tendency to an extremum which is not seen because of the limited wavelength range.

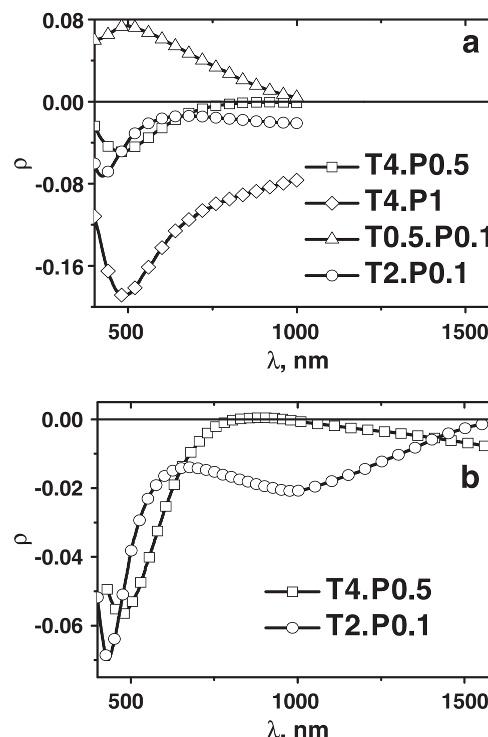

Fig. 4. a) The spectral dependence of the polarization difference ρ (λ) for the samples T4.P0.5, T4.P1, T0.5.P0.1, and T2.P0.1 measured at the incidence angle 55°; b) The same for the samples T4.P0.5 and T2.P0.1 in the extended spectral range.

The $\rho(\lambda)$ curves shown in Fig. 4 for the samples T4.P0.5 and T4.P1 (4 wt.% BADCT/0.5 and 1 wt.% PVAC in the initial solution, respectively) were re-plotted in Fig. 5 where they are shown in the traditional for resonance phenomena form. Besides, they are normalized to their maxima. As it might be seen, both curves perfectly coincide at the higher frequency side of the resonance $\omega_0 = 4.3 \cdot 10^{15}$ s^{-1}. This indicates the universal nature of the phenomenon in the considered frequency range. Since the samples are supposed to have the same tin dioxide content, it is reasonable to associate the coincidence of the resonance frequencies with the same number of the interacting with light centers. Since the frequency range in Fig. 5 is close to the saturation region of the dispersion dependence $\omega(k)$ describing the resonance phenomenon it can be concluded that the nature of that extremum is associated with the local plasmon resonance on cluster particles.

At the same time, the curves 1 and 2 in Fig. 5 are more complex than an elementary oscillator resonance function, which is schematically

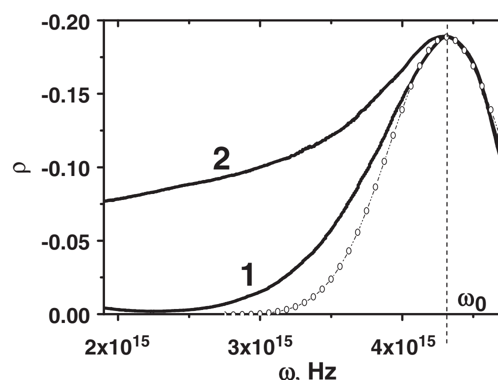

Fig. 5. Frequency dependencies of the parameter ρ for the samples T4.P0.5 and T4.P1 (curves 1 and 2, respectively) measured at the incidence angle 55°, recalculated from $\rho(\lambda)$ dependence shown in Fig. 4 and normalized for the maximum values. Open circles: Gaussian normal distribution function.

Author's personal copy

shown by the open circles at the same figure for frequencies smaller than ω_0. Such a discrepancy, in our opinion, can be attributed to the presence of another resonance electromagnetic interaction in the considered frequency range. It might be the excitation of plasmon–polariton waves associated with the intercluster dipole–dipole interaction in the film [20]. The conditions for their appearance and the degree of their manifestation depend, in contrast to the local resonance, not only on the total number of interacting centers, but also on the size, shape of clusters and the distance between them, as it is evidenced by many publications (e.g. [21]). This statement was confirmed by the resonance excitation of the surface plasmon wave that manifests itself by the extremum in the $\rho(\lambda)$ curve obtained for the sample T2.P0.1 (2 wt.% BADCT and 0.1 wt.% PVAC in the initial solution), see Fig. 4b around 950 nm. One can expect that this resonance, being spaced by a considerable distance from the local one, should be present even more significantly in the curves obtained for T4.P0.5 (curve 1) and T4.P1 (curve 2, Fig. 5), but for some reason it is overlapped with a local resonance, and this overlapping requires a separate study. The separation of the two resonances is problematic, unless the curves 1 and 2 in Fig. 5 show a second extremum or at least some non-monotonic behavior of the $\rho(\lambda)$ dependencies. One can suggest that this problem may be facilitated by calculating the difference between the actual resonance curves and the standard symmetrical curve (normal distribution), thus fulfilling a reconstruction of the SPR spectrum. However, such a procedure requires a justification.

The above method allows also the determination of the local plasmon resonance parameters. Indeed, under the condition that the elementary oscillator resonance curve matches the curve of the normal distribution function it becomes possible to determine not only the resonance frequency, but also, using its half-width, the relaxation time, which is estimated as $\gamma = 1.3 \cdot 10^{-14}$ s. For a comparison, the value of this parameter for the gold films with thickness d = 50 nm was reported as $\gamma_{Au} = 7.14 \cdot 10^{-13}$ s [22] that can indicate a high structural perfection of the metal film.

4. Conclusions

An application of the original technique for the SPR phenomena investigation by the methods of polarization modulation of electromagnetic radiation had confirmed the principle possibility to detect SPR in the conducting films of tin dioxide. (The preliminary data were reported in the publication [23]). The important tool of the used procedure is an investigation of the polarization difference ("anomalous reflection") function $\rho = R_s^2 - R_p^2$ which exhibits strong sensitivity to the film optical parameters. This property of ρ permitted to investigate the film structural properties. Particularly, the negative ρ sign reveals the metallic nature of light absorption in the films. But, as was established earlier by the authors [12], the angular range of the negative ρ and the shape of its angular dependence in the present case are very different for continuous and cluster films. Thus, the larger extent of the negative ρ angular range above the critical angle was exclusively related to the cluster structure of the material. In addition, the results obtained in this paper allow one, if an appropriate model is formulated, to reconstruct the cluster shapes. The information necessary for such a reconstruction may be obtained from the $R_s{}^2{}_{|sp}$ and $R_p{}^2{}_{|sp}$ value relation characterizing a degree of the resonance interactions on the basis of their angular and spectral dependencies. In particular, in case of the investigated SnO_2 films, the cluster shape anisotropy (non-sphericity) is evidenced by the non-equality of the films' effective parameters obtained for the s- and p-polarized radiation. However, further work is necessary for the full reconstruction of the cluster forms.

Therefore, the main conclusions of the present work are:

- Polarimetric technique was applied for investigation of surface plasmon resonances excited in SnO_2 films.
- Principle optical parameter of the film $\rho(\theta, \lambda)$ was measured, where $\rho = R_s^2 - R_p^2$ — reflection coefficient difference.
- It was established that $\rho(\theta, \lambda)$ is associated with SnO_2 film structure.
- $\rho(\theta, \lambda)$ amplitude is reported to be dependent on SnO_2 precursor concentrations.

Acknowledgments

The authors are much grateful to Dr. habil. Vladimir Chirvony (University of Valencia, Spain) for his high professional assistance in preparation of the manuscript for publication.

References

[1] M. Batzill, U. Diebold, Prog. Surf. Sci. 79 (2005) 47.
[2] In: D.S. Ginley, H. Hosono, D.C. Paine (Eds.), Handbook of Transparent Conductors, Springer Science + Business Media, New York, 2010.
[3] T.A. Miller, S.D. Bakrania, C. Perez, M.S. Wooldridge, in: Kurt E. Geckeler, Edward Rosenberg (Eds.), Functional Nanomaterials, American Scientific Publishers, Valencia, USA, 2006, p. 1.
[4] In: V.M. Agranovich, D.L. Mills (Eds.), Surface Polaritons: Electromagnetic Waves at Surfaces and Interfaces, North-Holland, Amsterdam, 1982, Nauka, Moscow, 1985.
[5] N.L. Dmitruk, V.G. Litovchenko, V.L. Strizhevskiy, Surface Polaritons in Semiconductors and Dielectrics, Naukova dumka, Kyiv, 1989.
[6] A. Otto, Z. Phys. 216 (1968) 398.
[7] E. Kretschman, Z. Phys. 241 (1971) 313.
[8] L.I. Berezhinskiy, L.S. Maximenko, I.E. Matyash, S.P. Rudenko, B.K. Serdega, Opt. Spectrosc. 105 (2008) 257.
[9] S.N. Jasperson, S.E. Schnatterly, Rev. Sci. Instrum. 40 (1969) 761.
[10] M. Born, E. Wolf, Principles of Optics, Cambridge University Press, Cambridge, 1999.
[11] E.A. Vinogradov, T.A. Leskova, A.P. Ryabov, Opt. Spectrosc. Rus. Acad. Sci. J. 76 (1994) 311.
[12] L.I. Berezhinskiy, O.S. Litvin, L.S. Maksimenko, I.E. Matyash, S.P. Rudenko, B.K. Serdega, Opt. Spectrosc. 107 (2009) 264.
[13] S. Singh, B.D. Gupta, Meas. Sci. Technol. 21 (2010) 115202.
[14] G. Fu, W. Cai, C. Kan, C. Li, L. Zhang, Appl. Phys. Lett. 83 (2003) 36.
[15] S. Cho, S. Lee, U.S. Oh, S.J. Park, W.M. Kim, B.K. Cheong, M. Chung, K.B. Song, T.S. Lee, S.G. Kim, Thin Solid Films 377–378 (2000) 97.
[16] L.N. Filevskaya, V.A. Smyntyna, V.S. Grinevich, in: Inter-universities Scientific Articles, 15, Astroprint, Odessa, 2006, p. 11.
[17] B. Ulug, H.M. Türkdemir, A. Ulug, O. Büyükgüngör, M.B. Yücel, V.S. Grinevich, L.N. Filevskaya, V.A. Smyntyna, Ukr. Chem. J. 7 (2010) 12.
[18] In: H.F. Mark, N.G. Gaylord, N.M. Bikales (Eds.), Thermogravimetric analysis to wire and cable coverings, Encyclopedia of Polymer Science and Technology, vol. 14, Interscience Publishers, New York, 1971, p. 149.
[19] M. Anastasescu, M. Gartner, S. Mihaiu, C. Anastasescu, M. Purica, E. Manea, M. Zaharescu, in: International Semiconductor Conference Proceedings, 1, 2006, p. 163.
[20] A. Evlyukhin, Lett. Russ. Acad. Sci. J. Exp. Phys. 31 (2005) 14.
[21] A.S. Shalin, S.G. Moyseev, Opt. Spectrosc. 106 (2009) 916.
[22] L.S. Maksimenko, I.E. Matyash, I.A. Minaylova, O.N. Mishchuk, O.N. Rudenko, B.K. Serdega, Opt. Spectrosc. 109 (2010) 808.
[23] B.K. Serdega, I.E. Matyash, L.S. Maximenko, S.P. Rudenko, V.A. Smyntyna, V.S. Grinevich, L.N. Filevskaya, B. Ulug, A. Ulug, B.M. Yucel, Semiconductor 45 (2011) 316.